# Automated Technique For Comparison Of Magnetic Field Inversion Lines With Filament Skeletons From The Solar Feature Catalogue

**6 authors**, including:

Stanley S. Ipson
University of Bradford
**107** PUBLICATIONS   **1,501** CITATIONS

SEE PROFILE

Valentina V. Zharkova
Northumbria University
**272** PUBLICATIONS   **2,933** CITATIONS

SEE PROFILE

S. Zharkov
University of Hull
**114** PUBLICATIONS   **1,355** CITATIONS

SEE PROFILE

Jean Aboudarham
Observatoire de Paris
**115** PUBLICATIONS   **712** CITATIONS

SEE PROFILE

Some of the authors of this publication are also working on these related projects:

Project   image watermarking for copyright protection View project

Project   Engineering System Design for Automated Space Weather Forecast View project

# AUTOMATED TECHNIQUE FOR COMPARISON OF MAGNETIC FIELD INVERSION LINES WITH FILAMENT SKELETONS FROM THE SOLAR FEATURE CATALOGUE

S. S. IPSON, V. V. ZHARKOVA, S. ZHARKOV and A. K. BENKHALIL

*Department of Cybernetics, Bradford University, Bradford, BD7 1DP, U.K.*
*(e-mail: v.v.zharkova@brad.ac.uk)*

and

J. ABOUDARHAM and N. FULLER

*LESIA, The Paris-Meudon Observatory, F92195 Meudon Principal Cedex, France*

**Abstract.** We present an automated technique for comparison of magnetic field inversion-line maps from SOHO/MDI magnetograms with solar filament data from the Solar Feature Catalogue created as part of the European Grid of Solar Observations project. The Euclidean distance transform and connected component labelling are used to identify nearest inversion lines to filament skeletons. Several filament inversion-line characteristics are defined and used to automate the decision whether a particular filament/inversion-line pair is suitable for quantitative comparison of orientation and separation. The technique is tested on 551 filaments from 14 Hα images at various dates, and the distributions of angles and distances between filament skeletons and line-of-sight (LOS) magnetic inversion lines are presented for six levels of magnetic field smoothing. The results showed the robustness of the developed technique which can be applied for a statistical analysis of magnetic field in the vicinity of filaments. The method accuracy is limited by the static filament detection which does not distinguish between filaments, fibrils, pre-condensations and filament barbs and this may increase the asymmetries in magnetic distributions and broadening in angular distributions that requires the incorporation of a feature tracking technique.

## 1. Introduction

Solar phenomena such as sunspots, filaments, flares and active regions vary with an 11-(22) year cycle, which is assumed to be connected with the behaviour of the solar magnetic field (e.g., Mackay and van Ballegooijen, 2001). The solar magnetic field measured with the line-of-sight (LOS) ground-based or space-based magnetographs (Babcock and Babcock, 1955; Scherrer *et al.*, 1995), or recent full-vector magnetographs (Wang *et al.*, 1998; Ulrich, 1992) provides an important data resource for understanding and predicting solar activity. The importance of the magnetic field has been emphasized in many theoretical works including the following: heating of the solar atmosphere; formation and support of multi-levelled magnetic loops and filaments resting on top of them; activation of energy releases in solar flares and coronal mass ejections; and in many other small- and large-scale events occurring in the solar atmosphere and interplanetary space.

This paper is concerned with fully automatic analysis of the data archived in the Solar Feature Catalogue generated by the European Grid of Solar Observations project (Zharkova *et al.*, 2005), in order to identify the relationships between magnetic field and solar filaments; specifically between the LOS magnetic inversion lines and solar filament skeletons (axes). Different scales of magnetic field magnitudes are assumed to account for solar events of different scales and these event scenarios result mostly from magnetic configurations of loops with opposite magnetic polarities. For example, solar filaments often appear on the boundaries of coronal holes (Kuperus and Raadu, 1974; Lerche and Low, 1980) or above a middle line between two-ribbon flares (Fox, McIntosh, and Wilson, 1998; McIntosh, 1979; Sturrock and Jardin, 1994; Grigoriev and Ermakova, 1999) that usually is very close to the location of magnetic inversion lines, or apparent magnetic neutral lines (AMNLs, or MNLs hereafter). Filaments are well established to be flux ropes with a longitudinal magnetic field (twisted or not) occurring above the bipolar magnetic regions in the vicinity of magnetic inversion lines (Kippenhahn and Schlüter, 1957; Hood and Priest, 1979; Priest, Hood, and Anzer, 1989; Démoulin and Priest, 1993; Rust and Kumar, 1994; Priest, van Ballegooijen, and Mackay, 1996).

Therefore, LOS magnetic observations were often used to mark the filament locations in many wavelengths (see, for example, Gaizauskas *et al.*, 1997; Grigoriev and Ermakova, 1999). However, it is apparent that filaments occurring at higher atmospheric levels in the chromosphere or corona should not necessarily match the photospheric inversion lines because of a possible different magnetic structure at these levels. In this case, magnetic observations at the photosphere can be brought up to higher atmospheric layers by smoothing, or averaging, the magnetic data within a particular window (Duvall *et al.*, 1977; Durrant, Kress, and Wilson, 2001). This smoothing results in a cancellation of smaller-scale magnetic fields, or smaller loops, and approximates higher magnetic structures. By repeating this smoothing process several times it is possible to find the degree of smoothing that allows matching the inversion-line maps with filament skeletons (Durrant, 2002). This technique was tested on many magnetic data from MWO and NSOKP for filament elongation not only in the solar centre but in polar plumes and polar crown gaps and revealed a very good agreement between the MNLs and filaments at various levels of smoothing (Durrant, 2002) and during different phases of the solar cycle (McCloughan and Durrant, 2002).

Hence, in order to extend this research to the data obtained in the Solar Feature Catalogue and to produce sufficient statistical analysis of the filaments and their locations with respect to MNLs in relation to the level of smoothing an automated technique is required. The preparation and preliminary analysis of the magnetic field inversion maps is described in Section 2.1 and the methodology used to extract quantitative comparative information about the filaments and their neighbouring inversion lines is described in Section 2.2. Some statistical results obtained from 14 days observations are then presented and discussed in Section 3 and finally conclusions are drawn in Section 4.

## 2. Description of the Techniques

Let us demonstrate the effect of magnetic field smoothing on the locations of MNLs with respect to filaments. An example of the superposition of automatically extracted filaments (Fuller, Aboudarham, and Bentley, 2005) and MNLs obtained using three different amounts of Gaussian smoothing is shown in Figure 1. It can be seen that there is a range of agreement between inversion lines and filament elongations, although the geometrical relationship between a filament and its nearest neighbouring inversion line is complicated in some cases. In general, with increasing smoothing, the association between filaments and inversion lines becomes stronger and the complexity of the inversion lines is reduced.
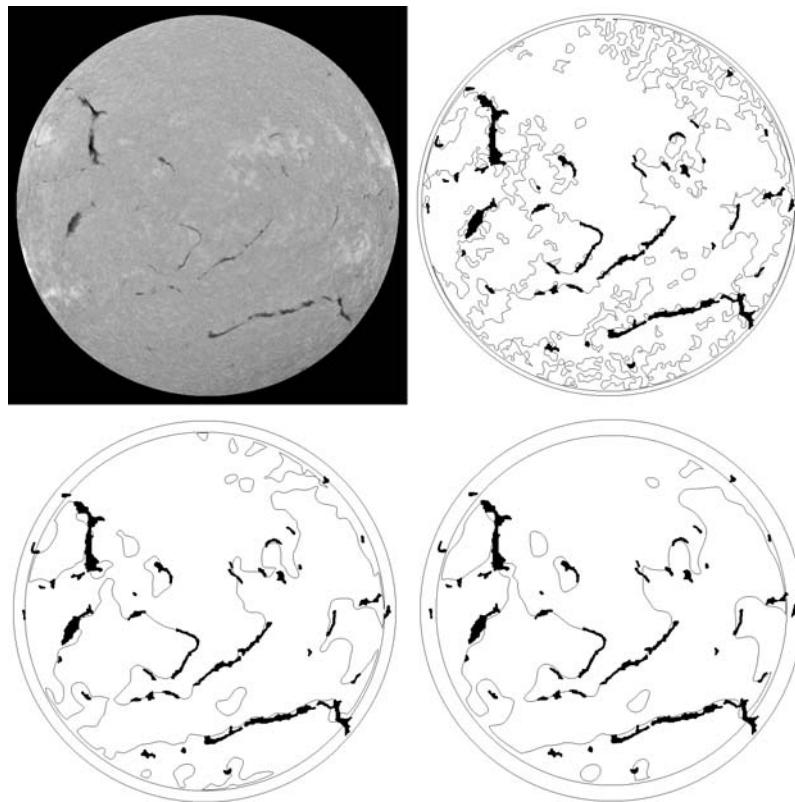


*Figure 1.* Filaments observed on 1 May 2002 in Hα radiation at the Meudon observatory. *Top left*: original observation after standardisation of size and limb darkening removal, *top right*: filaments (in black) detected at Meudon superimposed on inversion-line map generated from remapped SOHO magnetogram smoothed using Gaussian convolution kernel with standard deviation of 9″. *Bottom left and right*: smoothed with 22″ and 30″ kernels, respectively. The outer circles indicate the edge of the solar disk and the regions between the two circles are the invalid boundary regions influenced by the arbitrary field outside the disk.

In order to develop algorithms to quantify the relationship between filaments and inversion lines, we included observations of filaments during the solar maximum and solar minimum. As the sources of filament data, eight Hα solar images from the Meudon observatory were selected from the Solar Feature Catalogue entries for the maximum-activity years 2001 and 2002 and six were selected for the minimum-activity year 1997. These are just preliminary results obtained using a small database in order to identify a range of possible relationships the algorithm has to be compatible with that later can be implemented for a large SFC database.

### 2.1. PREPARATION OF MAGNETIC FIELD INVERSION MAPS

The parameters from the catalogue used are the chain code representations of the filament skeletons (filament boundaries are also available but were not used for automated comparison with inversion lines) defined on images standardised to a size of 1024 pixels × 1024 pixels with a centred solar disk of radius 420 pixels. The 14 SOHO MDI LOS magnetograms, which are closest in observation times to the Hα images were identified. Despite a limited accuracy of a few gauss for lower magnetic fields obtained from the SOHO/MDI measurements (Scherrer *et al.*, 1995), the MDI data are used for testing the technique because of their easy availability for every filament observation and high quality of the data that is free from atmospheric distortions. Moreover, the magnetic data smoothing required for the technique works towards reducing this error allowing us to use the MDI data. The developed technique is rather generic and applicable to any other magnetic data and can be applied to ground-based observations in the future.

The magnetograms are synchronised to the Hα observation times and position and simultaneously remapped to the standardized size of the corresponding Hα images. The resulting magnetograms are subjected to the following operations in order to produce the inversion-line maps for comparison with the corresponding filament maps.

1. A 2-D Gaussian smoothing filter with specified standard deviation is applied. Since this filter is separable, for faster execution, it is applied as a 1-D horizontal convolution followed by a 1-D vertical convolution, each with kernel width equal to five standard deviations of the Gaussian distribution.

2. Pixels in the smoothed magnetograms closest to points of magnetic field sign reversal are marked using the following procedure. Each pixel in the magnetogram is examined in turn for a change in sign in the horizontal, vertical and two 45° directions and the direction of the largest change noted. The pixel is marked as an inversion point if a change in sign exists and the linear interpolated position of the zero of the LOS magnetic field is nearer to the pixel than to its two neighbours in the direction of maximum change.

3. The pixels marking inversion points obtained by the previous procedure generally have more than two neighbouring points and to simplify the subsequent

automatic interpretation of the inversion-line data, the inversion point maps obtained in step 2 are subjected to the thinning procedure of Arcelli, Cordella, and Levialdi (1981). The resulting inversion point maps have most marked points falling on contiguous lines with only two marked neighbours per point and only rarely are points with one, or more than two, marked neighbours found.

4.  In order to simplify the subsequent automatic interpretation of the inversion maps, the maps obtained in step 3 are segmented to identify the different connected objects (Haralick and Shapiro, 1992). For example, in the bottom right image shown in Figure 1 there are nine separate inversion lines of which one is much larger than the others. This segmentation procedure uniquely labels pixels in each distinct object, records the dimensions of the rectangle bounding each object and records the number of pixels comprising each object. These connected objects mainly consist of continuous lines of varying lengths and complexities. As the degree of smoothing increases, the connected objects decrease in number and in complexity of shape. At the lower smoothing levels applied in the present work a significant number of objects which are judged too small to be associated with filaments are found and these are eliminated from the inversion point map at this stage to simplify the subsequent automatic interpretation procedure. The threshold for elimination of objects is not critical, and was set at objects comprising 50 points so, for example, only inversion lines comprising more than 50 connected points are shown in Figure 1.

## 2.2. THE METHODOLOGY FOR COMPARISON OF FILAMENTS AND MAGNETIC INVERSION LINES

It can be noted from Figure 1 that although, typically, there is a close association of filaments and magnetic inversion lines, the geometrical relationship between them can be rather complicated. Only in the simplest cases do filament skeletons lie close to and have very similar shapes to the inversion lines (first case). Sometimes a filament skeleton is close to a bow in an inversion line (second case) or different parts of a filament skeleton are closest to points on different, non-contiguous, inversion lines (third case). Occasionally, a filament skeleton is close to part of an inversion line that includes pixels with less than or more than two adjacent neighbours (fourth case). Examples of these cases are shown in Figure 2. Given this complexity, an automatic comparison system must be robust and capable of handling the wide variety of possibilities mentioned earlier.

The comparison between the filaments and the magnetic field inversion lines was simplified by taking into account only three points on each filament, namely, the two end points (which should be near the filament foot points) and the mid-point of the filament skeleton. The points on the magnetic field inversion lines which
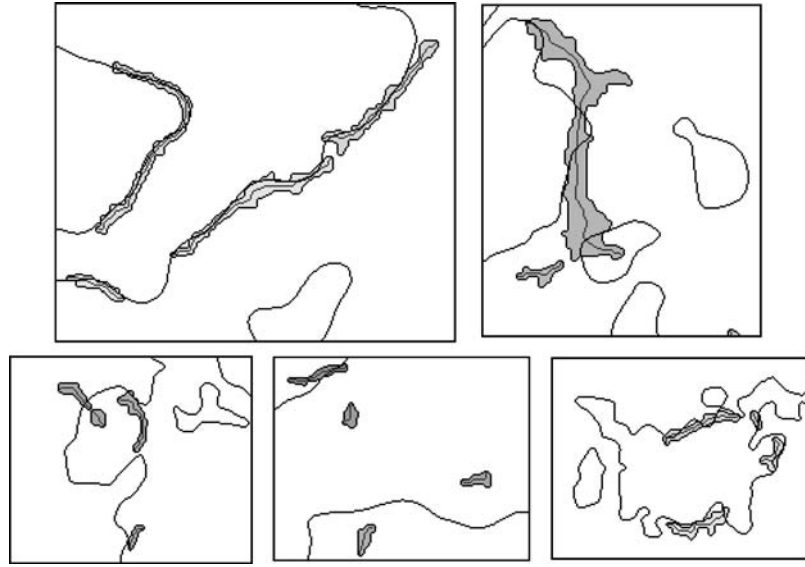
*Figure 2.* Example cropped images (all to same scale) showing five filament and inversion-line rela-
tionships. *Top row*: Hα observation on 1 May 2002 with 22″ smoothing, *left*: showing close agreement
between filament and inversion lines, *right*: showing two filaments both with opposite skeleton end
points closest two different inversion lines. *Bottom row*: Hα observation on 1 April 2002, *left*: with
22″ smoothing showing a filament sitting across the neck of the bow in an inversion line, *middle*: with
22″ smoothing showing three filaments with distances to inversion lines greater than their lengths,
*right*: with 9″ smoothing showing filament (top, large) close to an inversion line with a cross-over.

are closest to the filament points are determined. The mean of the three distances
between the points on the filament and the nearest neutral line points is used as a
measure of the filament to inversion-line separation. The angle between the straight
lines joining end points of a filament and the end points on the corresponding
inversion line is used as a measure of the angle between the filament and the neutral
line. Examples of filaments making large angles to the associated inversion line are
shown in Figure 3. Where possible, the number of pixels along the inversion line
between the identified end points is counted. The relationship between filament
and inversion lines is identified during the process of obtaining these measures and
conclusions drawn automatically as to the quality of the match between filament
and inversion line. The individual stages in this analysis are as follows.

   1. The filament objects in the filament map each consist of a boundary line and
      a skeleton line, which are separately labelled connected lines of pixels. Each
      pixel in a skeleton, apart from the two end pixels, has exactly two adjacent
      neighbours. Filament skeletons are detected by scanning through the filament
      map pixel by pixel. When a skeleton pixel is found, a line tracking procedure
      is invoked which finds the start, middle and end pixels and records their pixel
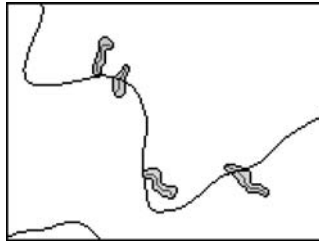
*Figure 3.* Examples of filaments observed on 1 April 2002 near the centre of the solar disk aligned at large angles to the nearest inversion line obtained with 22″ smoothing. From left to right, the computed angles between the filaments and the inversion line are 65°, 67°, 7° and 50°, respectively.

co-ordinates in a list. The tracking procedure labels all pixels in a skeleton as visited and the scanning continues until all the pixels in the map have been tested for non-visited filament skeleton pixels.

2. In order to locate the points on inversion lines which are closest to the start, middle and end points of filament skeletons a Euclidean Distance Map (EDM) of the magnetic field inversion map is constructed. The EDM defines for each pixel not on an inversion line the horizontal and vertical offsets to the nearest point on an inversion line. It is generated using the algorithm described by Cuisenaire and Macq (1999). A list of co-ordinates of the inversion-line point nearest to the filament skeleton start, middle and end points is created by applying the appropriate offsets, stored in the EDM to the start, middle and end co-ordinates of the filament skeletons. This list also includes with each inversion-line point the unique label associated with the inversion line during the segmentation stage. Examples of start, middle and end points defined by this procedure are shown in Figure 4. It is now possible to determine whether or not the inversion-line points identified as being closest to a filament are on the same inversion line. For comparisons between the inversion lines and filaments, the mean distance between the three corresponding filament and inversion points are used as a measure of the filament to inversion-line distance. The angle between the straight lines joining the start and end points for the filament and the corresponding inversion line are used as a measure of the difference in angular alignment between filament and inversion line.

3. If the three inversion-line points associated with a filament are on the same inversion line then an inversion-line tracking procedure is invoked to determine the number of pixels (length) on the line between the three points. Because in practice the start, middle and end points on the inversion line, named by their association with the corresponding points on a filament may not be in this order on the inversion line, the inversion-line tracking procedure starts from the middle pixel and tracks outwards alternately one pixel at a time in both directions until it has reached both start and end points.
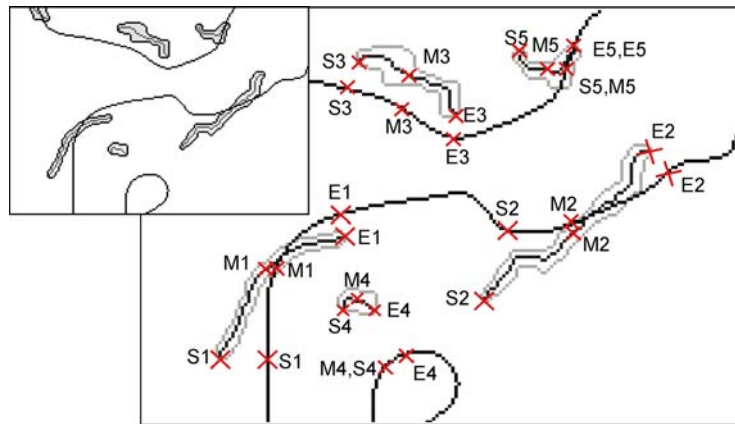
*Figure 4.* Cropped image of filaments and inversion lines on 5 July 2002 with magnified view showing the start (S), middle (M) and end (E) points defined on numbered filaments and the corresponding nearest points on inversion lines. In the cases of filaments 4 and 5 the inversion-line points nearest to the filament start and middle coincide and also in the case of filament 5 the filament end point is on the inversion line so that filament and inversion-line end points are coincident.

This ensures the procedure will reach both start and end points irrespective of whether they are on the same or opposite sides of the middle point. In the former case, the length returned is the larger of the middle to start or middle to end numbers and in the latter case it is the number of pixels between the start and end points. Filament numbers 4 and 5 in Figure 4 are examples of cases where the start and middle points correspond to the same point on the inversion line and more extreme cases do arise in practice where start and end inversion-line points are both on the same side of the middle inversion-line point. During the tracking procedure, a check is made of the number of touching inversion points and, if this differs from two, then the procedure stops and records the situation before continuing with the next filament.

4. Using the information assembled in steps 1–3, a filament is classified as being in a quantifiable relationship with an inversion line or not. Five different situations have been identified for the latter case, namely: (i) the three inversion points associated with a filament are not all on the same inversion line; (ii) the filament to inversion-line distance is greater than the length of the filament; (iii) the length of the inversion-line segment associated with a filament is more than twice the length of the filament; (iv) during tracking of the inversion-line segment associated with a filament a point with only one or more than two neighbours was encountered; (v) one or more of the filament points or the three associated inversion-line points are within half the width of the convolution kernel from the edge of the solar disk and are thus in the region not correctly defined. Examples of the cases (i) to (iv) are shown in Figure 2 and examples of case (v) in Figure 1.

## 3. The Results and Discussion

The comparisons of the results extracted from the Solar Feature Catalogue (Fuller, Aboudarham, and Bentley, 2005) are presented in Figures 5(a)–7(a) and 8–10 for 217 filaments detected at the solar maximum in the Hα images from the Meudon observatory captured on 17 March 2001, 26 April 2001, 2 May 2001 and 26 July 2001 for the magnetic field smoothing kernel with standard deviations of about 9–30″ (half widths ranging from 10 to 35 pixels). Figure 5 shows the histograms of angles between the filament skeletons (axis) taken from the SFC and the magnetic inversion lines for the Hα images taken in 2001 (a) and 2002 (b). The histograms of distances between filament skeletons and inversion lines are presented in Figure 6 and the histograms of average LOS magnetic fields at filaments are presented in
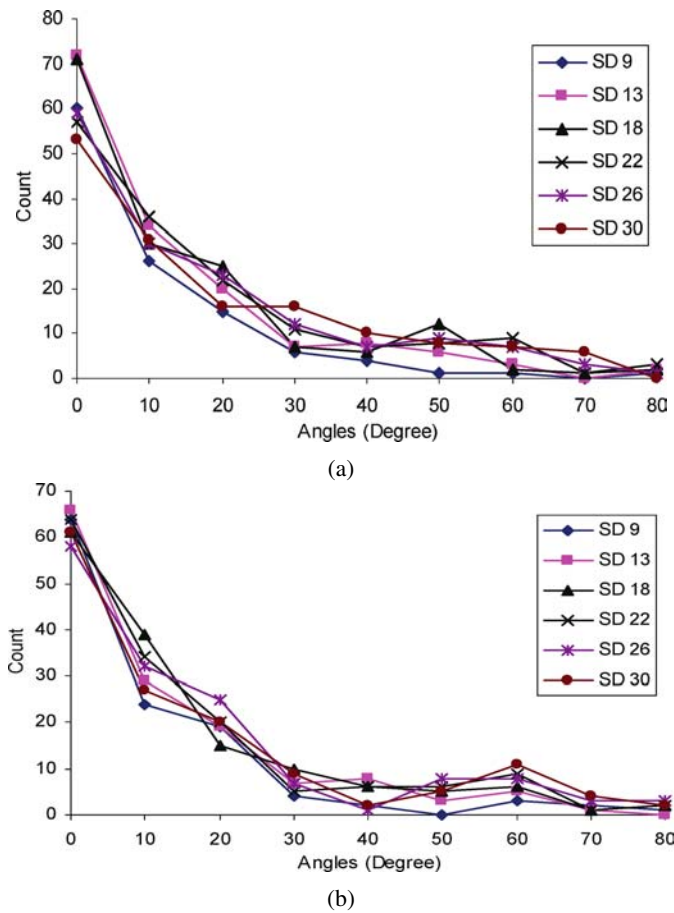


(a)

(b)

*Figure 5.* (a) Histograms of angles between filaments and neutral lines for smoothing kernels with standard deviations of 9 – 30″ (half widths 10 – 35 pixels in steps of 5 pixels), from Hα images taken in 2001. (b) Histograms of angles between filaments and neutral lines for smoothing kernels with standard deviations of 9 – 30″ (half widths 10 – 35 pixels in steps of 5 pixels), from Hα images taken in 2002.
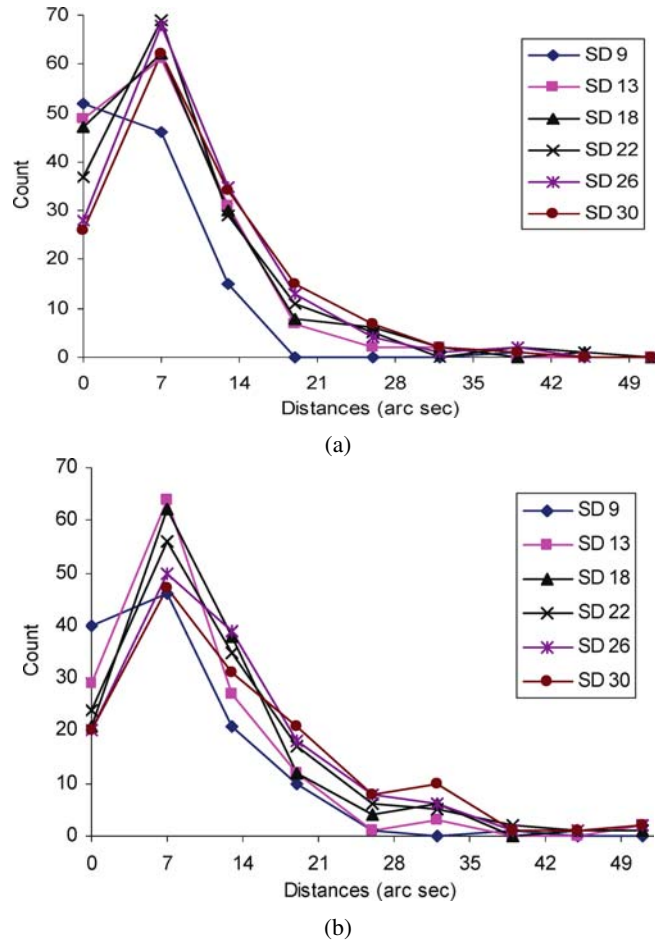
(a)



(b)

*Figure 6.* (a) Histograms of distances (in arc sec) between filaments and neutral lines for smoothing kernels with standard deviations of $9-30''$ (half widths $10-35$ pixels in steps of 5 pixels), from H$\alpha$ images taken in 2001. (b) Histograms of distances (in arc sec) between filaments and neutral lines for smoothing kernels with standard deviations of $9-30''$ (half widths $10-35$ pixels in steps of 5 pixels), from H$\alpha$ images taken in 2002.

Figure 7 for the same dates as in Figure 5. Figures 8–10 show the data taken from all the images in Figures 5(a)–7(a), respectively, divided into four bands of latitude by lines at $0°$ and $\pm30°$.

In order to test the reliability of the results, Figures 11–13 show pairs of histograms for the filaments located less than and greater than $30°$ from the disk centre for angles, distances and magnetic fields respectively, for 207 filaments detected on 1 April 2002, 9 April 2002, 1 May 2002 and 5 July 2002. Figures 14–19 present similar data to those in Figures 5–10 for 127 filaments detected on 1 March 1997, 1 April 1997, 1 June 1997, 24 July 1997, 3 August 1997 and 3 September 1997, which was a year of the minimum solar activity.
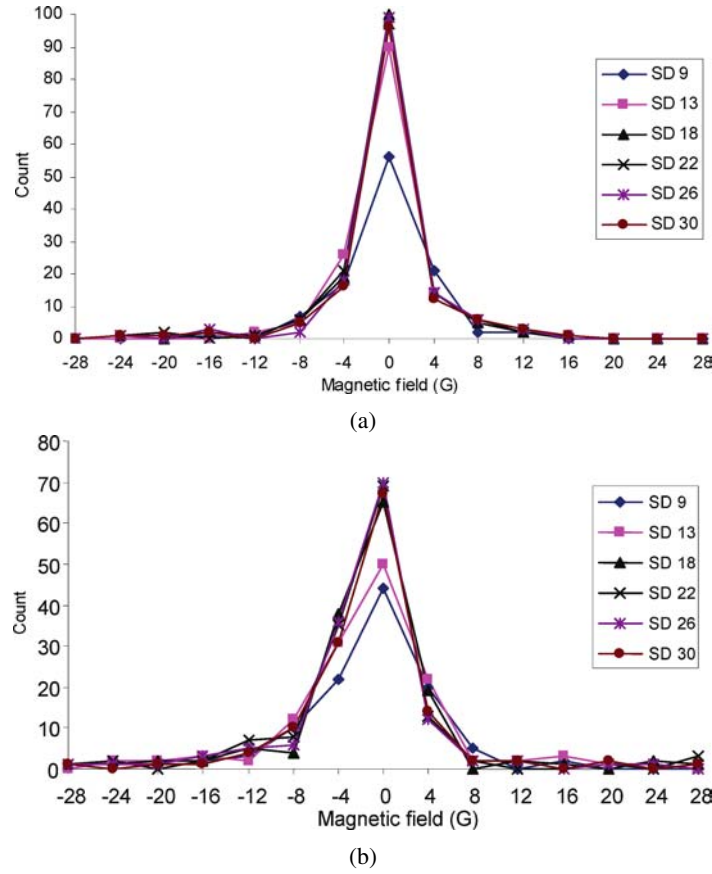
(a)



(b)

*Figure 7.* (a) Histograms of magnitudes of line-of-sight magnetic fields in gauss at filaments for smoothing kernels with standard deviations of $9 - 30''$ (half widths $10 - 35$ pixels in steps of 5 pixels), from H$\alpha$ images taken in 2001. (b) Histograms of magnitudes of line-of-sight magnetic fields in gauss at filaments for smoothing kernels with standard deviations of $9 - 30''$ (half widths $10 - 35$ pixels in steps of 5 pixels), from H$\alpha$ images taken in 2002.

In all the graphs, only the filament detections which are not rejected by the criteria listed under item 4 of Section 2.2 are included. The number of rejected filaments, for different amounts of smoothing and different years are shown in Table I. In the case of the 2002 data, the number of rejected filaments varies from 88 to 60 for the smoothing kernels of $9 - 30''$, respectively, from a total of 207 pixels. Six of these rejected filaments are small, have large magnetic field intensities and are likely to be sunspots that are misclassified as filaments. It is also possible that some of the smaller features detected as filaments are fibrils/spicules, pre-condensations or filament barbs that are not distinguished by the static filament detection technique. Hence, for a reliable interpretation of such data in the future we need to introduce a feature tracking method that will allow us to investigate the filament dynamics (and track pre-condensations) and to eliminate the features,

TABLE I

The variation in number of filaments ignored with amount of smoothing applied to magnetograms for the observations analysed in years 2002, 2001 and 1997.

|  | Smoothing | | | | | | |
|---|---|---|---|---|---|---|---|
|  | 9″ | 13″ | 18″ | 22″ | 26″ | 30″ | Total number of filaments |
| Ignored 2002 | 88 | 69 | 62 | 60 | 62 | 66 | 207 |
| Ignored 2001 | 103 | 65 | 61 | 63 | 66 | 70 | 217 |
| Ignored 1997 | 72 | 63 | 55 | 52 | 53 | 60 | 127 |
| Total | 263 | 197 | 178 | 175 | 181 | 196 | 551 |

The last column on the right shows the number of filaments observed in each year for the days included in the analysis. The bottom row shows the total number of filaments ignored for each amount of smoothing and the total number of filaments included in the analysis.
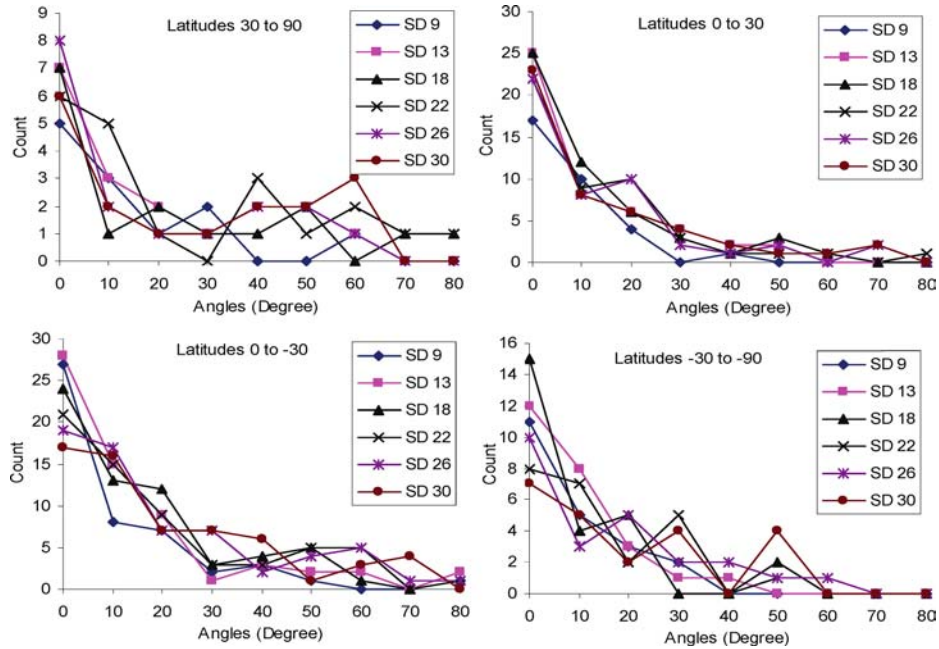


*Figure 8.* Histograms of filament to inversion-line angle separated into four bands of latitude for smoothing kernels with standard deviations of $9-30''$ (half widths $10-35$ pixels in steps of 5 pixels), from H$\alpha$ images taken in 2001.

which do not belong to filaments (fibrils/spicules or filament barbs). In the case of the 2001 data, the number of rejected filaments varies from 103 to 61 from a total of 217 and in the case of the 1997 data, the number of rejected filaments varies from 72 to 52 from a total of 127. A very small degree of smoothing results in
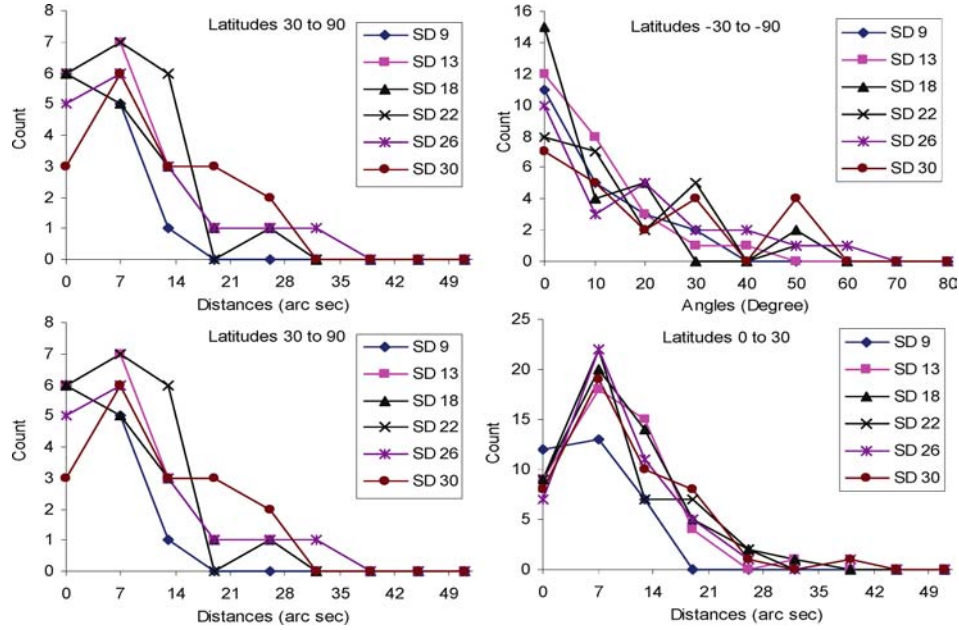
*Figure 9.* Histograms of filament to inversion-line distances separated into four bands of latitude for smoothing kernels with standard deviations of $9-30''$ (half widths $10-35$ pixels in steps of 5 pixels), from H$\alpha$ images taken in 2001.
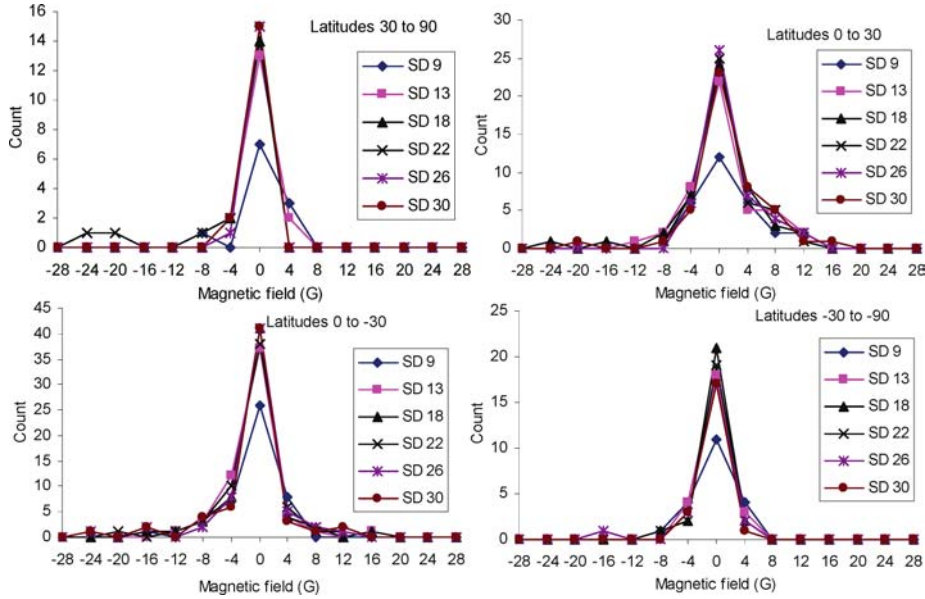


*Figure 10.* Histograms of magnitudes of line-of-sight magnetic fields in gauss at filaments separated into four bands of latitude for smoothing kernels with standard deviations of $9-30''$ (half widths $10-35$ pixels in steps of 5 pixels), from H$\alpha$ images taken in 2001.
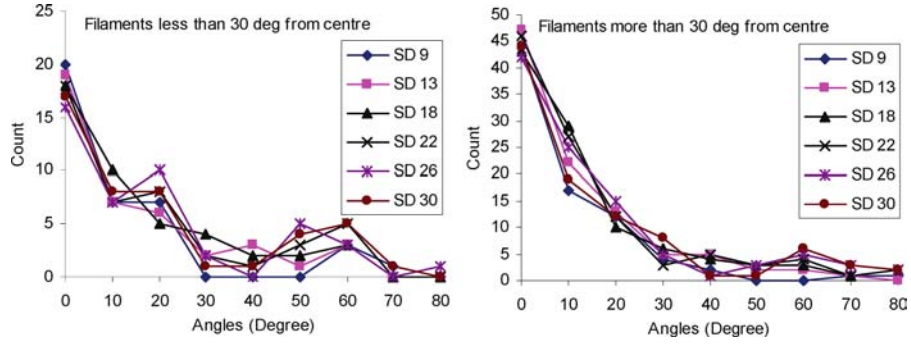
*Figure 11.* Histograms of the filament to inversion-line angle for smoothing kernels with standard deviations of $9-30''$ separated into two groups, less than or greater than $30°$ from the disk centre, from H$\alpha$ images taken in 2002.
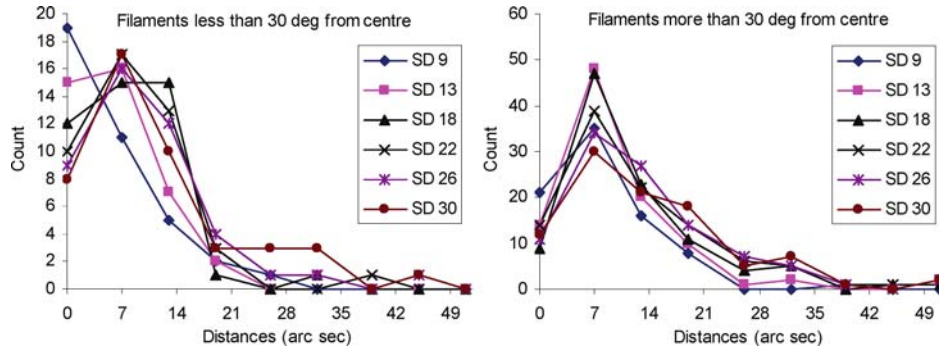


*Figure 12.* Histograms of filament to inversion-line distance for smoothing kernels with standard deviations of $9-30''$ separated into two groups, less than or greater than $30°$ from the disk centre, from H$\alpha$ images taken in 2002.
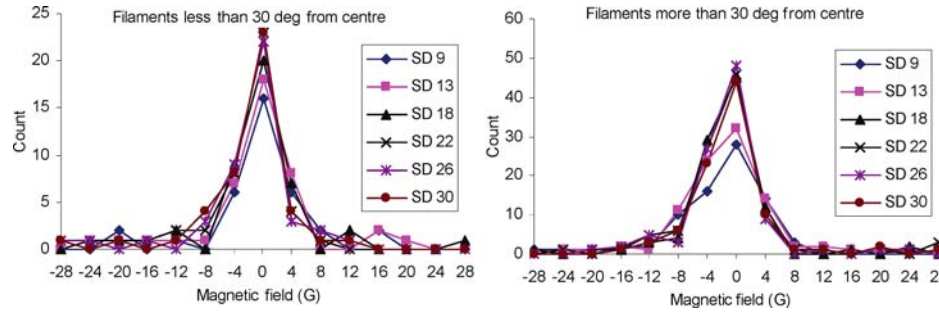


*Figure 13.* Histograms of filament to inversion-line magnetic fields in gauss for smoothing kernels with standard deviations of $9-30''$ separated into two groups, less than or greater than $30°$ from the disk centre, from H$\alpha$ images taken in 2002.
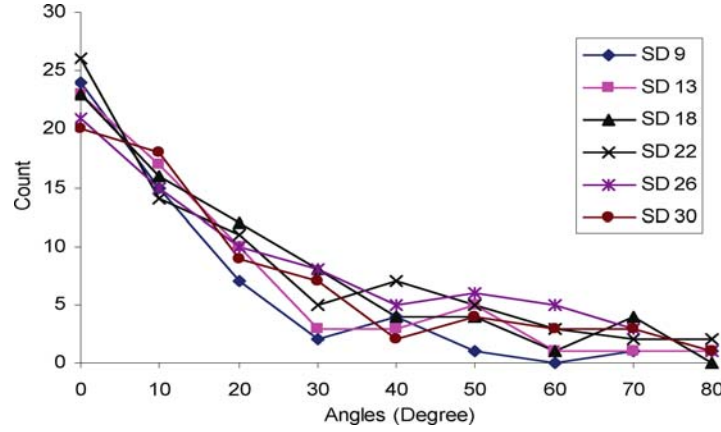
*Figure 14.* Histograms of angles between filaments and neutral lines for smoothing kernels with standard deviations of $9-30''$ (half widths $10-35$ pixels in steps of 5 pixels), from an H$\alpha$ image taken on 1 March 1997.
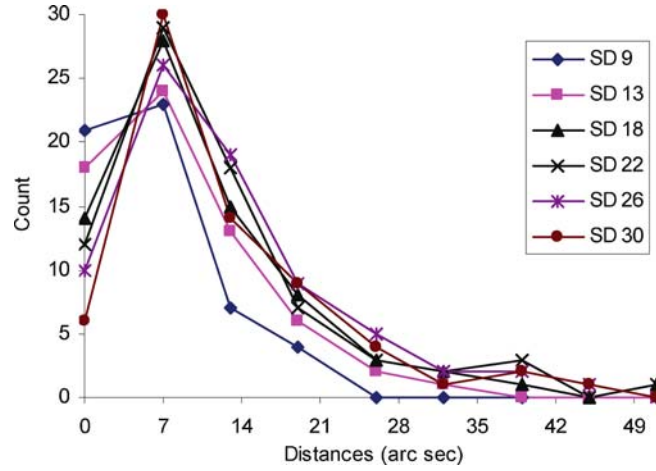


*Figure 15.* Histograms of distances (in arc sec) between filaments and neutral lines for smoothing kernels with standard deviations of $9-30''$ (half widths $10-35$ pixels in steps of 5 pixels), from an H$\alpha$ image taken on 1 March 1997.

a large number of complex inversion lines and then all filaments are likely to be rejected because of the criterion that the ends of the filament are close to the same inversion line so that an angle between the two can be defined. In line with this, for the data presented, the rejection rate is largest for the smoothing kernel of $9''$ and rather similar for the remaining degrees of smoothing, although it is lowest for the smoothing kernel of $18''$ and $22''$. The fraction of filaments rejected in the 2002 and 2001 data is about 28% and in the 1997 data the fraction is about 41%. This is associated with increased complexity of the magnetic field data in 1997
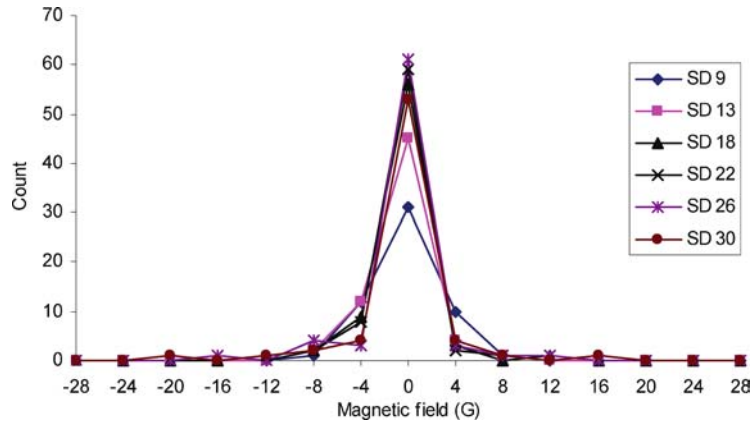
*Figure 16.* Histograms of magnitudes of line-of-sight magnetic fields in gauss at filaments for smoothing kernels with standard deviations of $9 - 30''$ (half widths $10 - 35$ pixels in steps of 5 pixels), from an H$\alpha$ image taken on 1 March 1997.



*Figure 17.* Histograms of filament to inversion-line angle separated into four bands of latitude for smoothing kernels with standard deviations of $9 - 30''$ (half widths $10 - 35$ pixels in steps of 5 pixels), from H$\alpha$ images taken in 1997.

compared with in 2001 and 2002. For example, with smoothing of $22''$, for the six observations used in 1997 the average number of inversion lines per observation is 31 compared with 14.5 in 2001 and 13 in 2002. The average total inversion line length per observation is also greater with a total of 10 644 pixels in 1997 and
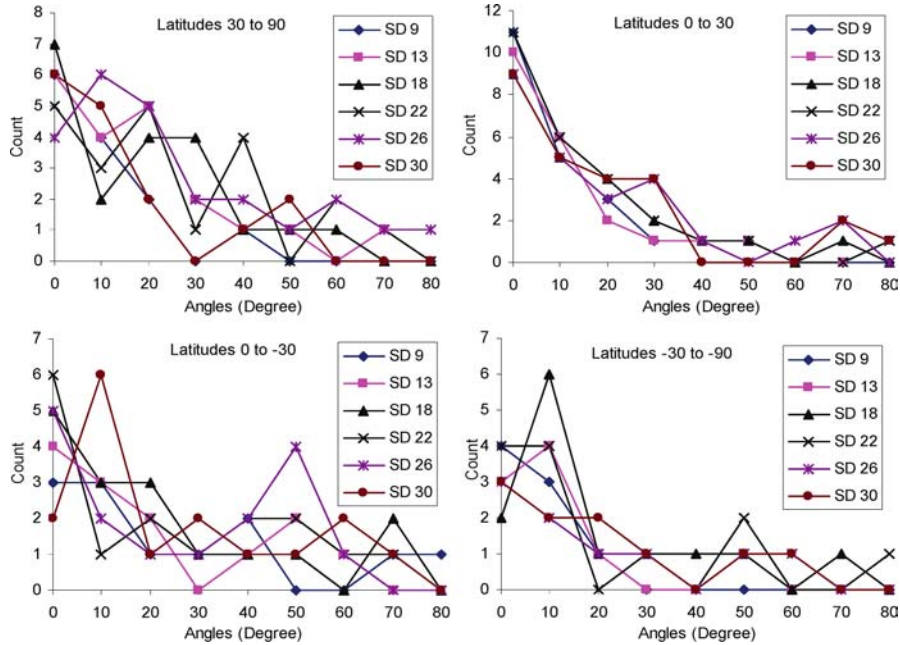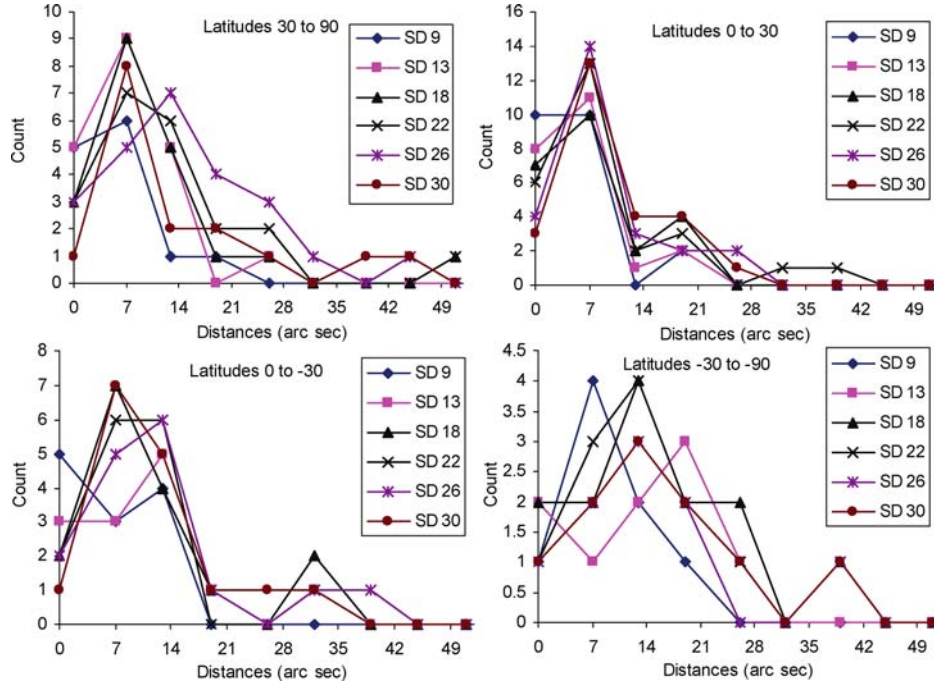
*Figure 18.* Histograms of filament to inversion-line distances separated into four bands of latitude for smoothing kernels with standard deviations of $9 - 30''$ (half widths $10 - 35$ pixels in steps of 5 pixels), from H$\alpha$ images taken in 1997.

7724 and 6511 in 2001 and 2002 respectively. The results presented for years 2002 and 2001 are now discussed first in detail and then compared with the results for 1997.

The distribution of angles (Figure 5) for all smoothing kernels is largest at $0°$, falling towards zero with a half width about $15°$. There is evidence of an extended tail or secondary broad peak centred at about $50°$. The main peak in the distributions for the unsmoothed magnetic field and its angle to a filament skeleton is rather similar to the results obtained with the Hanle effect measurements by Leroy (1977, 1978) in prominences who measured the distributions of angles between the prominence long axis and a horizontal magnetic field with the full magnetic field vector for 16 quiescent prominences. In the present study, we measure a LOS magnetic field that is in most cases a vertical component unless close to the limb. However, by measuring the angle between the long axis of a filament and the inversion line we are likely to measure a deviation of the filament magnetic field from a horizontal one in the direction perpendicular to the plane of observation similar to those measured by Leroy (1978) in prominences that is believed to lead to rather similar results.

Additionally, there is evidence for the main peak narrowing and the secondary peak increasing in amplitude with the increase of magnetic smoothing (Figure 5).
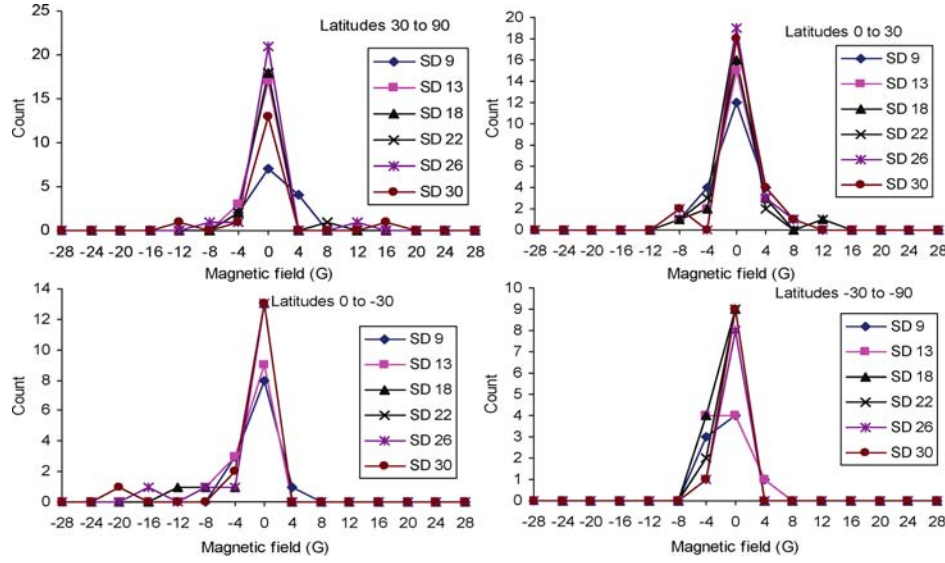
*Figure 19.* Histograms of magnitudes of line-of-sight magnetic fields in gauss at filaments separated into four bands of latitude for smoothing kernels with standard deviations of $9-30''$ (half widths $10-35$ pixels in steps of 5 pixels), from H$\alpha$ images taken in 1997.

The distribution of angles for 2002 (Figure 5b) shows a more prominent secondary peak with centre about $55°$ than those for 2001. The closer elongation of MNLs along the filament skeletons can suggest that the increasing magnetic smoothing to produce the inversion lines better matching the filament locations corresponding to their higher altitudes above the photosphere (Durrant, 2002). The latter, i.e. a secondary peak in the angles, needs to be checked with more statistics, since the number of filaments is rather small. However, if this is correct, then it suggests that with the increasing altitude there is a small increase in number of filaments making large angles with the inversion line that possibly can be flagging a magnetic configuration misbalance and needs to be investigated with both more observations, to have a reliable statistics and advanced theoretical models. This will be the scope of a future paper.

A distribution of the MNL distances from the filament skeletons (Figure 6) displays a single peak in both years 2001 and 2002, which has a maximum at about $10''$ and a full width about $18''$ falling to lower magnitudes at about $40''$. This can be a reflection either of an inclination of magnetic loops on the top of which the filaments are located (Priest, 1984; Démoulin and Priest, 1993) or of a magnetic field non-potentiality, or its helicity, that is reflected in a shift of a vertical magnetic field component observed in the current comparison.

If the increase of magnetic smoothing effectively decreases the heights of filaments above the estimated inversion lines, so one can expect a decrease in the distance for filaments sitting directly above the inversion lines. However, in Figure 6

it appears that the number of filaments with the smallest distance, on the contrary, decreases with the increase of magnetic smoothing and with increased smoothing, the width of the peak appears to increase as well. This can be accounted for by the increasing helicity of magnetic lines (larger loop cross-sections), while reaching higher altitudes in the solar atmosphere. Alternatively, the expected effect may be masked by the variable statistics for the filaments indicated in Table I.

The distribution of magnetic field magnitudes (Figure 7) displays a single peak with a maximum at zero and a full width of about 6 G. For the current observations in 2001 the peak is nearly symmetric and although filaments with the fields of $-4$ G are more numerous than the filaments with fields of $+4$ G, i.e. the number of filaments with negative magnetic fields is about 100% larger than the number of filaments with positive fields. This is in some agreement with the measurements by Leroy (1977) of the distribution of the magnetic field intensity in prominences, which was found to peak about 3.5 G. The asymmetry towards negative magnitudes becomes more noticeable for 2002 (see Figure 7(b)). There is also some evidence that the number of filaments in the distribution peaks around a zero magnitude and increases with the increased magnetic smoothing (compare the different curves in Figure 7). This is consistent with the fact that by applying the increasing magnetic smoothing one estimates the inversion lines at higher altitudes in the solar atmosphere, giving a better agreement with the filaments (Durrant, 2002).

The results shown in Figures 5–7 for 2001 have been also used for the distributions for four bands of latitude presented in Figures 8–10, respectively. The total number of filaments are about 18 in the band of $30-90°$, about 48 in the $0°$ to $+30°$ band, about 62 in the $0°$ to $-30°$ band, and about 25 in the $-30°$ to $-90°$ band. From a comparison of Figures 5–7 and 8–10 it can be seen that the dispersion in these distributions is increased compared with those shown in Figures 5–7.

Despite the limited statistics used in the tests of the developed technique, we can produce some preliminary conclusions. For instance, the magnetic field distributions are slightly asymmetrical in the two equatorial bands (particularly the $0-30°$ band), which obviously reveals in filaments the noticeable vertical components of magnetic field measured in the central areas of the solar disk unlike the horizontal ones measured closer to the limb. The equatorial magnetic distributions are slightly broader than the polar distributions. In all latitude bands, the magnetic field distributions peak at $0$ G for all levels of smoothing. These results emphasize that there are some latitudinal and, possibly, longitudinal variations in filament magnetic fields, which are connected to the activity centres on the solar surface similar to those suggested by McCloughan and Durrant (2002), which are to be checked in the future on more reliable filament statistics.

In order to ensure the obtained statistics do not depend on a projection effect for the LOS magnetic field measurements, in Figures 11–14 we compare the statistical results for 2002 obtained for the region near the solar centre (under $30°$) and in the rest of the solar disk. Obviously, a greater number of filaments is located at bigger angles than $30°$ from the disk centre compared with the number of filaments

closer to the centre reflecting the difference of a factor of about 3 between the relevant disk areas. It can be seen that the distribution of filament angles (Figure 11) and distances (Figure 12) closer to the centre are wider than those towards the limb, which is opposite to what is expected from the projection effects. By inspecting Figure 11 one can see signs of a secondary maximum at 55° in both bands. Figure 12 shows the distributions of filament to inversion-line distances revealing that in the disk centre the maximum of filaments are elongated to the MNLs for the smallest smoothing of 9″ moving to a distance of about 7″ for those filaments in the outer band. This can reflect the filament projection onto the solar disk for the calculations of the magnetic imbalance for these filaments. Magnetic field distributions shown in Figure 13 reveal significant asymmetries for both bands: in the disk centre and outside with the asymmetry being higher in the outer band that is obviously increased by the projection effect. Hence, we can conclude that the projection effect for LOS magnetic field slightly distort but does not change significantly the main features of the filament statistics presented earlier.

Now, let us compare the results for the solar maximum in 2001 (Figures 5–10) and 2002 (Figures 5(b)–7(b)) with the results in 1997 about the solar minimum shown in Figures 14–19. The number of filaments included in the high-activity years are 217 and 207, whereas the number of filaments included in 1997 is 127, despite the larger number of observations, because the activity is lower. Apparently, there are many similarities, in general, with more differences in details showing a wider distribution dispersion in 1997, possibly, because of a lower number of filaments during the minimum.

The angle distributions in Figures 5, 11 and 14 have similar shapes with the same evidence of a small secondary maximum at larger angles. The width of the principal peak starting at 0° is wider in the 1997 data than the 2001 and 2002 data by about 50%. All the distributions show evidence of the peaks shifting to a larger angle with the increasing smoothing and the peaks in the 1997 data are about 25% broader than the corresponding peaks in the 2001 and 2002 data. All magnetic field distributions in Figures 7, 13 and 16 have peaks at 0 G, but the asymmetry present in the 2002 data is reduced to a difference of about 50% in the 2002 data and to about zero in the 1997 data.

The angle, distance and magnetic field distributions of filaments in 1997 for the four bands in latitude are plotted in Figures 17–19. In the 1997 data, the total number of filaments from north to south are about 20, 25, 15 and 10, respectively, indicating a shift of the maximum number from the southern to the northern 30° equatorial band in 1997. From a comparison of Figures 17–19 and 14–16 it can be seen that the dispersion in these distributions is again increased compared with those shown in 2001 due to the lower number of filaments.

By comparing the statistical results for all 3 years, 1997, 2001 and 2002, we can conclude that the distributions of magnetic field are strongly asymmetric in 2002 (at all latitudes although not shown) and close to symmetric at all latitudes in 1997.

The asymmetry becomes smaller in 2001 compared to 2002 and it is positive in the $0 - 30°$ band and negative in the other three bands. These results need to be checked in the future with more reliable filament statistics over a more extended range of the solar cycle.

## 4. Conclusions

In the current paper, we present some preliminary results of an automated comparison of solar filament elongations extracted from the Solar Feature Catalogues and LOS magnetic inversion lines detected using the software tools written in Microsoft C. The technique was tested on 551 automatically detected filaments from 14 Meudon observatory H$\alpha$ images for three different years obtained from the Solar Feature Catalogue. The presented distributions have been automatically obtained, for the first time as far as we are aware, for measures of filament to inversion-line separation, filament to inversion-line angle and filament magnetic field intensities and for different degrees of magnetic smoothing with standard deviations ranging from about $9 - 30''$.

For all smoothing kernels the distribution of angles between a filament skeleton and MNL is largest at $0°$, falling towards zero with a half width about $15°$. There is a secondary small broad peak centred at about $60°$. There is also some evidence for the main peak narrowing and the secondary peak increasing in amplitude with an increase of magnetic smoothing, which supports the assumption that filaments are better co-aligned with higher magnetic structures that are achieved with a wider window of smoothing (Durrant, 2003).

A distribution of the MNL distances from the filament skeletons displays a single peak, which has a maximum at about $7''$ and a full width about $18''$ falling to lower magnitudes at about $40''$. The number of filaments with the smallest distance decreases with the increase of magnetic smoothing and with increased smoothing the width of the peak appears to increase as well.

The 2002 distributions for filaments located nearer and further than $30°$ from the disk centre shows that the properties of the angle and distance distributions are not associated with projection effects, since they are present in the near centre distributions. On the other hand, the magnetic field asymmetry observed in the 2002 distributions is more marked in the far from centre distributions and so may be influenced by projection effects.

The distribution of magnetic field magnitudes displays a single peak with a maximum at zero and a full width of about 6 G. For the current observations in 2002 the peak is clearly asymmetric and filaments with the fields of $-4$ G are about twice as numerous as the filaments with fields of $+4$ G. The results for 2001 show lesser asymmetry and the results for 1997 are nearly symmetric. The distributions in 2002 are in fact asymmetrical at all latitudes, and this asymmetry is greater in the two equatorial bands, particularly the $0°$ to $-30°$ band, than in the two polar

bands. The equatorial magnetic distributions are also more than twice as wide as the polar distributions.

Because only 551 filament detections are included in the current test research, it is rather difficult to identify clear trends in the reported filament characteristics with increased smoothing. However, in future research, we intend to apply these procedures to much larger numbers of such observations in order to improve the statistics and to ensure a sufficient reliability of the established and, possibly, new relationships with the new type of data. In addition, it has to be noted that the current static filament detection technique recognises some smaller features as filaments while they can be fibrils/spicules, pre-condensations or filament barbs. Hence, in the future, we need to introduce a feature tracking method that will allow us to investigate filament dynamics (and track pre-condensations) and to eliminate the features, which do not belong to filaments (fibrils/spicules or filament barbs). This data will provide additional information for the theories of solar filament formation and support during the whole solar cycle that can be used for better understanding of the nature of solar activity.

## Acknowledgements

## References

Arcelli, C., Cordella, L. P., and Levialdi, S.: 1981, *IEEE Trans. Patt. Anal. Machine Intell.* **PAMI-3-2**, 134.
Babcock, H. V. and Babcock, H. D.: 1955, *Astrophys. J.* **121**, 349.
Cuisenaire, O. and Macq, B.: 1999, in *Proceedings of the IEEE International Conference on Acoustics*, Speech and Signal Processing (ICCASSP99), Phoenix, AZ, Vol. 6, p. 3293.
Démoulin, P. and Priest, E. R.: 1993, *Solar Phys.* **144**, 283.
Durrant, C. J.: 2002, *Solar Phys.* **211**, 83.
Durrant, C. J., Kress, J. M., and Wilson, P. R.: 2001, *Solar Phys.* **201**, 57.
Duvall, T. L., Wilcox, J. M., Svalgaard, L., Scherrer, P. H., and McIntosh, P. S.: 1977, *Solar Phys.* **55**, 63.
Fox, P., McIntosh, P. S., and Wilson, P. R.: 1998, *Solar Phys.* **177**, 375.
Fuller, N., Aboudarham, J., and Bentley, R. D.: 2005, *Solar Phys.* **227**, in press.
Gaizauskas, V., Zirker, J. B., Sweetland, C., and Kovacs, A.: 1997, *Astrophys. J.* **479**, 448.
Grigoriev, V. M. and Ermakova, L. V.: 1999, *Astron. Astrophys. Trans.* **17**, 355.
Haralick, R. M. and Shapiro, L. G.: 1992, *Robotic Vision*, Addison Wesley, New York.
Hood, A. W. and Priest, E. R.: 1979, *Solar Phys.* **64**, 303.
Kippenhahn, R. and Schlüter, A.: 1957, *Z. Astrophysik* **43**, 36.

Kuperus, M. and Raadu, M. A.: 1974, *Astron. Astrophys.* **31**, 189.

Lerche, I. and Low, B. C.: 1980, *Solar Phys.* **66**, 303.

Leroy, J. L.: 1977, *Astron. Astrophys.* **60**, 79.

Leroy, J. L.: 1978, *Astron. Astrophys.* **64**, 247.

Mackay, D. H. and van Ballegoouen, A. A.: 2001, *Astrophys. J.* **560**, 445.

McCloughan, J. and Durrant, C. J.: 2002, *Solar Phys.* **211**, 53.

McIntosh, P. S.: 1979, UAG Report 70, World Data Centre for SIP, Boulder, Colorado.

Priest, E. R.: 1984, *Geophysics and Astrophysical Monographs*, Reidel, Dordrecht.

Priest, E. R., Hood, A. W., and Anzer, U.: 1989, *Astrophys. J.* **344**, 1010.

Priest, E. R., van Ballegooijen, A. A., and Mackay, D. H.: 1996, *Astrophys. J.* **460**, 530.

Rust, D. M. and Kumar, A.: 1994, *Solar Phys.* **155**, 69.

Ruždjak, V. and Tandberg-Hanssen, E.: 1990, *Lecture Notes in Physics*, Vol. 363, p. 317.

Scherrer, P. H., *et al.*: 1995, *Astron. Astrophys.* **2**, 363.

Sturrock, P. A. and Jardin, M.: 1994, *Book Review: Plasma Physics*, Cambridge University Press, Cambridge.

Ulrich, R. K.: 1992, *Astronomical Society of the Pacific*, San Francisco, California, p. 265.

Wang, H., Denker, C., Spirock, T. *et al.*: 1998, *Solar Phys.* **183**, 1.

Zharkova, V. V., Aboudarham, J., Zharkov, S., Ipson, S. S., Benkhalil, A. K., and Fuller, N.: 2005, *Solar Phys.*, this issue.